Journal of the Ceramic Society of Japan, Supplement 112-1, PacRim5 Special Issue, 112 [5] S658-S662 (2004)

Paper

Behavior of Li in $LiMn_2O_4$ Structure: Molecular Dynamics Study

Kenji TATEISHI, Douglas du BOULAY* and Nobuo ISHIZAWA*

Interdisciplinary Graduate School of Science and Engineering, Tokyo Institute of Technology, 4259, Nagatsuta, Midori, Yokohama 226-8502, Japan

**Ceramics Research Laboratory, Nagoya Institute of Technology, 10-6-29 Asahigaoka, Tajimi 507-0071, Japan*

Molecular dynamics (MD) was used to study ionic conduction processes in mixed valence compound $LiMn_2O_4$. The evolution of three different Mn valence distribution models was examined. For two models, I and II, the ideal spinel structure was adopted with randomly assigned valences. For model II the Mn valences were periodically randomly altered while preserving overall charge neutrality. In the third simulation, III, a charge ordered Mn valence model resembling the observed low temperature $LiMn_2O_4$ phase was adopted. Model I reproduces structural characteristics of the ideal spinel well, exhibiting modest Li ion self-diffusion. In model II the Li diffusion was greatly enhanced and in the charge ordered model III almost no diffusion was observed at all. Model II therefore reproduces the observed physical properties of the high temperature cubic spinel phase best, strongly supporting a Mn valence electron hopping model. Structural distortion indices were also calculated confirming that Li diffusion from the ideal tetrahedral LiO_4 environment is strongly associated with tetrahedral distortion.

[Received August 4, 2003; Accepted November 20, 2003]

Key-words : *Lithium manganese spinel, Molecular dynamics simulations, Rechargeable lithium ion batteries, Self-diffusion, Structural disorder*

Introduction

$LiMn_2O_4$ and related materials are promising candidates for cathode materials of rechargeable lithium ion batteries. However, $LiMn_2O_4$ has a problem in that its capacity for Li intercalation and deintercalation falls rapidly with repeated charge/discharge cycles. To some extent the problem is alleviated by partially substituting Mn with other metals M (M = Li, Co, Cr, Ni, Mg and Ga).[1)-4)]

$LiMn_2O_4$ is believed to be a mixed valence compound comprised of two distinct Mn^{3+} and Mn^{4+} species in equal proportions, presenting a first order structural phase transition around 290 K.[5)-9)] This transition results from partial charge ordering on the octahedrally coordinated Mn sites.[10)] The high temperature (HT) phase adopts a cubic spinel structure of symmetry $Fd\bar{3}m$ ($a = 8.24$ Å, Li: 8*a*, Mn: 16*d*, O: 32*e*) with no preferred ordering between Mn^{3+} and Mn^{4+} sites. EXAFS measurements suggest that distinct Mn^{3+} and Mn^{4+} ions coexist with distinctly different Mn^{3+}-O and Mn^{4+}-O bonding environments.[11)] At low temperature (LT) a preferred charge ordering mechanism arises lowering the symmetry to orthorhombic with space group *Fddd* ($3a \times 3a \times a$).

Using synchrotron powder X-ray diffraction, Ishizawa *et al.* observed significant residual electron density associated with the ideal Li and O atoms sites of the HT phase,[12)] implying a statistical distribution of atoms displaced from the ideal 8*a* and 32*e* sites. This model was supported by MD calculations which showed that such O atom displacements were strongly dependent on the valence of the coordinating Mn atoms and that the Li atom displacements were in turn dependent on the distribution of their coordinating O atoms.[13),14)]

Concerning the Li ion dynamics affecting the performance of batteries, it is becoming more apparent that it is closely correlated to electron hopping between Mn^{3+} and Mn^{4+} ions. Verhoeven *et al.* reported from NMR experiments of $Li[Mn_{1.96}, Li_{0.04}]O_4$ that Li is present at 8*a*, 16*c* and 16*d* sites and that Li diffusion occurs in the HT phase but not the LT phase.[15)] They indicated that Li ion dynamics and charge ordering on Mn sites are correlated. Also, it was recently demonstrated using MD simulations that self-diffusion of Li atoms is greatly facilitated by changes of Mn valences as a function of time.[14)]

Here our objectives were to use MD simulations to reveal the correlation between structural disorder, especially LiO_4 tetrahedral distortion, and Li ion dynamics in more detail. In addition to the three Mn charge distribution models, another MD potential function and parameters[17)] were assessed.

Experimental

MD simulations were carried out using the MXDORTO program developed by Kawamura.[18)] The pair potential function used primarily in this study was of Gilbert-Ida type:[19)]

$$U(r_{ij}) = \frac{Z_i Z_j e^2}{r_{ij}} + f_0(b_i + b_j) \times \exp\left[\frac{(a_i + a_j - r_{ij})}{b_i + b_j}\right]. \quad (1)$$

Here Z_i is the effective charge, e is the elementary electric charge, r_{ij} is the interatomic distance, f_0 is a constant (4.1868 $kJ \cdot mol^{-1} \cdot Å^{-1}$), and a_i and b_i represent the size and stiffness parameters, respectively. The first and second terms in Eq. (1) represent Coulomb interaction and short-range repulsion, respectively. The potential parameters used here are those derived by Suzuki *et al.*[16)]

Simulations were made assuming three distinct models: I) a model in which the arrangement of Mn valences does not change with respect to time, II) a model in which the arrangement of Mn valences changes with time preserving overall charge neutrality and III) a model in which Mn valences are charge ordering in the same manner as the LT phase.

Model I contained 512 Li, 512 Mn^{3+}, 512 Mn^{4+} and 2048 O atoms in a cubic MD cell with a dimension of 33.004 Å, being comprised of 64 ideal $LiMn_2O_4$ spinel unit cells. The Mn^{3+} and Mn^{4+} atoms were randomly assigned to the $Fd\bar{3}m$ 16*d* sites as initial configurations. Periodic boundary conditions were applied in all directions. Atomic motions and Coulomb interactions were calculated using the Verlet algorithm[20)] and Ewald method,[21)] respectively. A temperature of 300 K was simulated using an NTP ensemble at 2 fs intervals for 320 ps by controlling the atomic velocities and cell parameters.

The simulations of model II were identical to model I except

that the effective Mn charges were redistributed randomly at 40 ps intervals after an initial 100 ps structural relaxation phase. Overall charge neutrality was maintained.

Model III contained 216 Li, 240 Mn^{3+}–like,[10] 192 Mn^{4+} and 864 O atoms in a rectangular MD cell with dimensions of $24.7435 \times 24.8402 \times 24.5967$ Å^3 corresponding to $1 \times 1 \times 3$ of the *Fddd* unit cell. The effective charges of Mn^{3+}–like were modified from $+1.4$ (Mn^{3+}) to $+1.5$ in order to preserve charge neutrality.

Results and discussion

The vast amounts of atomic position and velocity data amassed in MD simulations are greatly simplified via statistical methods such as time and spatial averaging. **Figure 1** shows the displacement frequency distributions $P(\Delta x)$, $P(\Delta y)$ and $P(\Delta z)$ accumulated for all Li atoms in the extended *P*1 symmetry MD cell used for model I. For each Li atom, its displacement is measured with respect to the idealized 8*a* sites averaged over the extended pseudo-cubic lattice. Figure 1 shows that each of the displacement frequency distributions $P(\Delta x)$, $P(\Delta y)$ and $P(\Delta z)$ is strongly maximized at zero displacement so that on average the MD cell strongly resembles the $Fd\bar{3}m$ symmetry cell. In contrast, displacement frequencies accumulated for individual Li atoms such as those for Li1 and Li2 shown inset in Fig. 1, exhibit relatively sharp Gaussian-type profiles maximized away from their associated ideal 8*a* sites.[13] **Figure 2** shows a schematic diagram of two atoms vibrating harmonically about positions around 0.16 Å from their respective 8*a* sites. Although two Gaussian-type profiles maximized away from their respective 8*a* sites, the spatial superposition of those leads to a non-Gaussian-type single profile maximized at zero displacement. The frequency distribution accumulated for all Li atoms shown in Fig. 1 is precisely a superposition of this kind and is completely analogous to the time and spatial averaging that occurs during an X-ray diffraction experiment. Analogous mean displacements were also observed for the O atoms associated with their respective 32*e* sites. The implications are that although the time and spatially averaged $LiMn_2O_4$ structure strongly resembles a lattice with $Fd\bar{3}m$ symmetry, locally the structure is disordered.

The model I displacement distributions shown in Fig. 1 contain additional information about local maxima centered about 0.8 Å from the 8*a* sites along x, y and z. This is better illustrated by **Fig. 3** showing the frequency distribution of all Li atoms translated and rotated to a similar orientation in a $(\bar{1}10)$ plane and accumulated over 10000 steps ($100 < t < 120$ ps). This figure shows that over the duration of the MD simulation, Li have migrated away from the 8*a* tetrahedral sites and become localized near the 16*c* octahedral vacancies. The analogous distribution for model III is presented in **Fig. 4**, showing that a charge ordered model strongly impedes Li diffusion.

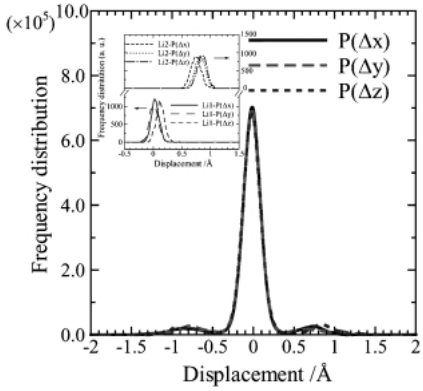

Fig. 1. Frequency distribution of all Li atoms as a function of the displacements Δx, Δy, Δz from initial positions.

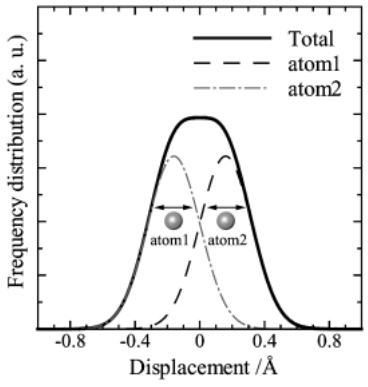

Fig. 2. Schematic diagram of two atoms vibrating harmonically about the positions around 0.16 Å away from their ideal sites.

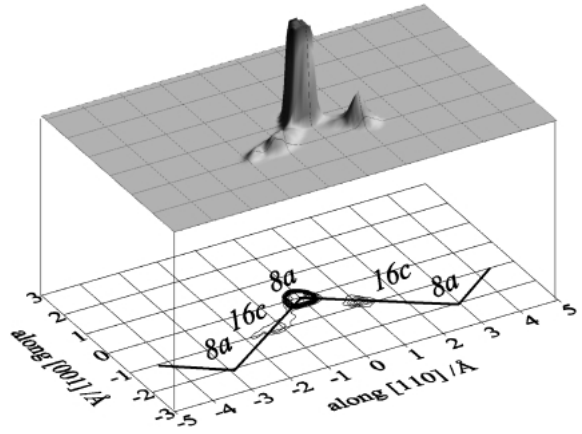

Fig. 3. Frequency distribution of all Li atoms on $(\bar{1}10)$ plane obtained from model I.

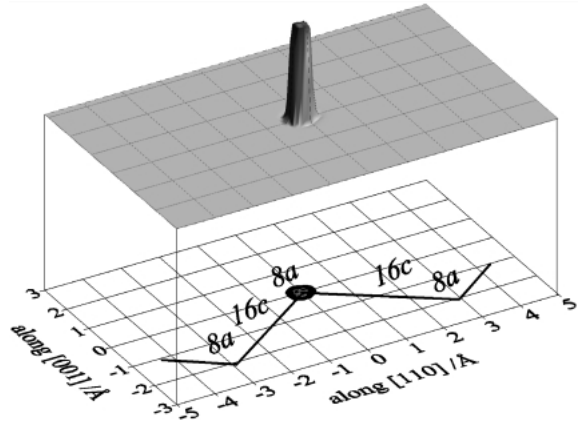

Fig. 4. Frequency distribution of all Li atoms on $(\bar{1}10)$ plane obtained from model III.

For the HT spinel phase each tetrahedral 8*a* site is coordinated by 4 O atoms which are in turn coordinated by 3 Mn and 1 Li atoms. Because there are many different combinations in which Mn^{3+} and Mn^{4+} valences can be assigned to the 12 coordinating Mn atoms, there is a similarly large number of LiO_4 tetrahedral distortion modes. Each apical O atom shifts to adopt a local equilibrium position compatible with its particular configuration of Mn^{3+}–O and Mn^{4+}–O bond lengths. This is different for the LT phase in which the Li atoms are located at 8*a*, 16*e*, 16*f* and 32*e* of *Fddd*. The charge ordered arrangement of second nearest neighbor Mn atoms means that only four tetrahedral distortion modes can occur. In model I the O atom displacements from their ideal positions were larger than those observed in model III suggesting that relatively large tetrahedral distortion is required to initiate Li ion migration beyond the tetrahedral constraints.

Although the model I MD simulation was run for up to 300 ps, after the initial 100 ps structural relaxation phase no further Li migration was observed. For model II on the other hand, after each 40 ps interval the spontaneous reassigment of Mn valence was followed by subsequent Li migration. **Figure 5** shows the planar distribution frequency accumulated for model II, showing that some Li migrated as far away as their nearest neighbor 8*a* sites and even a very small fraction as far as the second nearest neighbor 16*c* sites.

The MD simulations clearly suggest that Mn valence dependent LiO_4 tetrahedral distortion is required to initiate Li ion migration in the HT spinel phase. It is reasonable to expect that relatively large tetrahedral distortions are needed, possibly only occurring transiently as the lattice relaxes after each spontaneous charge reassignment.

From the MD data several distortion indices (DI) were calculated to quantify the degree of LiO_4 tetrahedral distortion. They were defined as follows:[22]

$$DI(MO) = \frac{1}{N}\sum_{i=1}^{N}\left(\frac{MO_i - MO_m}{MO_m}\right)^2 \qquad (2)$$

$$DI(OO) = \frac{1}{N}\sum_{i=1}^{N}\left(\frac{OO_i - OO_m}{OO_m}\right)^2 \qquad (3)$$

$$DI(OMO) = \frac{1}{N}\sum_{i=1}^{N}\left(\frac{OMO_i - OMO_m}{OMO_m}\right)^2 \qquad (4)$$

where MO_i represents the individual distances from the 8*a* site to oxygen atom, OO_i the individual lengths of the tetrahedral edges, OMO_i the individual angles O–8*a*–O and *m* signifies the mean value. For regular tetrahedra the DI values are zero. Indices for four tetrahedra that experienced Li ion migration, for example, are given in **Table 1**. Values were calculated for periods both before and after the Li ions migrated. The data show that DI values tend to increase after the Li escapes, presumably reflecting a degree of instability of an unoccupied O_4 tetrahedron. For reference, DI values averaged about all LiO_4 and unoccupied O_4 tetrahedra are also given in Table 1. In a previous study,[14] it was found that when Li atoms migrate, the tetrahedral O_3 faces through which Li atoms pass form bottlenecks which should be larger than the critical radius of 1.97 Å. That is the sum of conventional ionic radii[23] (O^{2-}: 1.38 Å, Li^+: 0.59 Å). By taking into account these results, it is presumed that Li ion diffusion is only favorable when tetrahedral distortion is relatively large and one of the bottlenecks is larger than the critical radius.

The results described above and in previous work[13),14] using a Gilbert-Ida type potential function are quite consistent with experimental observations. To examine the sensitivity of the MD simulations to the nature of the potential we also adopted a Born-Mayer-Buckingham type potential with parameters reported by other authors.[17] The Born-Mayer-Buckingham type function is as follows:

$$U(r_{ij}) = Z_i Z_j e^2/r_{ij} + A_{ij}\exp\left(-\frac{r_{ij}}{\rho_{ij}}\right) - \frac{C_{ij}}{r_{ij}^6}. \qquad (5)$$

Here A_{ij} and ρ_{ij} are the coefficients used for the short-range repulsion in the second term, and C_{ij} are those used for the Van der Waals interaction in the third term. Formal charges are assumed for Z_i in the first term representing Coulomb interaction. The shapes of the two potential functions of Li–O are illustrated in **Fig. 6**. The Gilbert-Ida type Li–O interatomic potential presents a steeper barrier rising rapidly at greater separations than the Born-Mayer-Buckingham type leading to a potential minimum at slightly longer radial separation for the former function.

The model I MD simulation was repeated using the Born-Mayer-Buckingham type potential. The resultant planar Li displacement distribution is shown in **Fig. 7**. The distribution

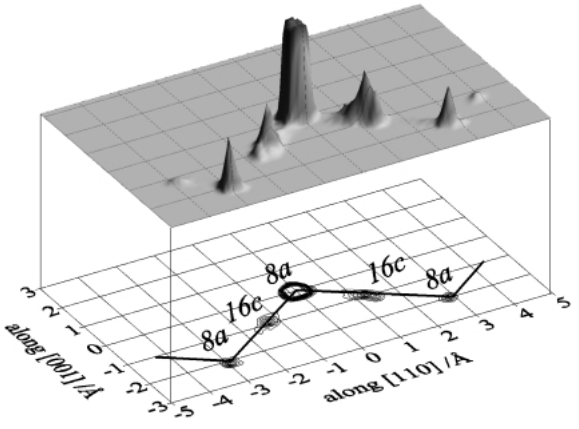

Fig. 5. Frequency distribution of all Li atoms on $(\bar{1}10)$ plane obtained from model II.

Table 1. Distortion indices of tetrahedra 1–4 and total average for all tetrahedra in model II

tetrahedra	Li	DI(MO)	DI(OO)	DI(OMO)
1	occupied	0.0020	0.0026	0.0043
	unoccupied	0.0030	0.0012	0.0029
2	occupied	0.0020	0.0023	0.0057
	unoccupied	0.0085	0.0024	0.0060
3	occupied	0.0032	0.0012	0.0041
	unoccupied	0.0053	0.0035	0.0049
4	occupied	0.0043	0.0013	0.0019
	unoccupied	0.0075	0.0055	0.0037
average	occupied	0.0024	0.0024	0.0038
	unoccupied	0.0051	0.0040	0.0047

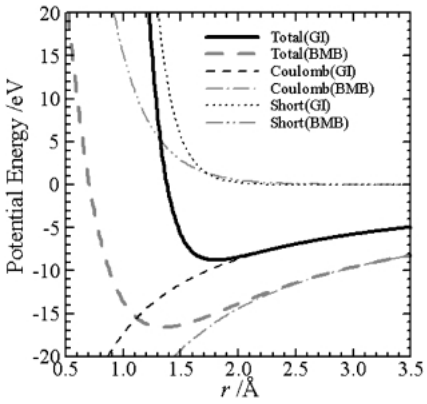

Fig. 6. Gilbert-Ida type (GI) and Born-Mayer-Buckingham type (BMB) potential functions of Li-O used for MD calculations.

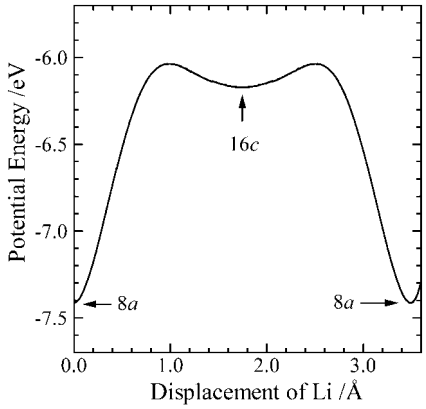

Fig. 8. Potential energy profile of Li along 8*a*–16*c* tie line in λ-MnO_2 assuming Gilbert-Ida type potential function.

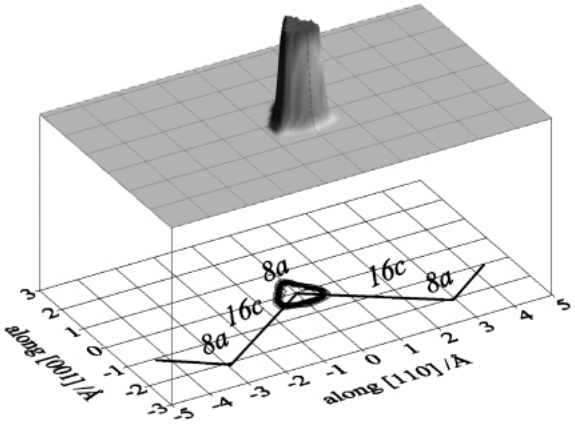

Fig. 7. Frequency distribution of all Li atoms on ($\bar{1}10$) plane obtained from model I using Born-Mayer-Buckingham type potential function.

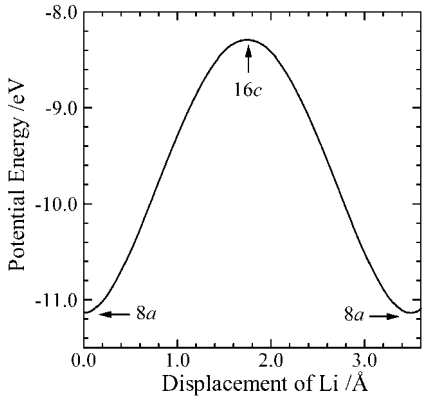

Fig. 9. Potential energy profile of Li along 8*a*–16*c* tie line in λ-MnO_2 assuming Born-Mayer-Buckingham type potential function.

of Li atoms around the 8*a* site is much broader than that determined using the Gilbert-Ida type potential and shown in Fig. 3. The averaged displacement of Li atoms from initial positions is 0.36 Å in the former while that of the earlier Gilbert-Ida type study was 0.16 Å. The shape of the Born-Mayer-Buckingham type potential is primarily responsible for the broader Li distribution, it having a broader but deeper and more strongly attractive potential well. Figure 7 also shows that no Li could migrate to the neighboring 16*c* sites, even during the initial structural relaxation.

We assumed a structural model in which a Li atom exists in λ–MnO_2 ($Li_xMn_2O_4$, $x=0$) and calculated the potential energy of a Li atom along the 8*a*–16*c* tie lines using both Gilbert-Ida type and Born-Mayer-Buckingham type potential functions. Potential energies were shown as a function of the displacement from initial 8*a* site in **Fig. 8** and **Fig. 9**. For both potentials the 8*a* site is most stable, but only for the Gilbert-Ida type potential there is a metastable saddle point at the 16*c* site. Because experiments have suggested that Li atoms also occupy at positions close to the 16*c* sites, we believe that a Gilbert-Ida type potential is better suited to reproduce the distribution and dynamics of Li in $LiMn_2O_4$ spinel.

Conclusion

Our MD calculations reproduce both the structural and dynamical features revealed by experiments without inconsistency. Li ion dynamics is strongly correlated with the distribution and rate of change of Mn valence. When Mn valences remained invariant, Li atoms were distributed around both 8*a* and 16*c* sites but self-diffusion seldom occurred after the initial structural relaxation period. When the Mn valences were charge ordered, Li remained locked at the 8*a* sites. Appreciable self-diffusion of Li atoms only occurred when the distribution of Mn valences was periodically adjusted reflecting an electron hopping model. The self-diffusion of Li was greatly facilitated when the bottlenecks formed by the LiO_4 tetrahedral faces were distorted to an extent larger than a critical radius of 1.97 Å.

Acknowledgment We are grateful to Prof. Katsuyuki Kawamura, Department of Earth and Planetary Sciences, Tokyo Institute of Technology, for kindly supplying us his MXDORTO program. This study was supported by Grant-in-Aid for Scientific Research on Priority Areas (B) (No. 740) from The Ministry of Education, Science, Sports and Culture of Japan. DDB acknowledges JSPS fellowship P02148.

References

1) Gummow, R. J., de Kock, A. and Thackeray, M. M., *Solid State Ionics*, Vol. 69, pp. 59–67 (1994).
2) Sigala, C., Guyomard, D., Verbaere, A., Piffard, Y. and Tournoux, M., *Solid State Ionics*, Vol. 81, pp. 167–170 (1995).
3) Guohua, L., Ikuta, H., Uchida, T. and Wakihara, M., *J.*

Electrochem. Soc., Vol. 143, pp. 178–182 (1996).
4) Pistoia, G., Antonini, A., Rosati, R. and Bellitto, C., *J. Electroanal. Chem.*, Vol. 410, pp. 115–118 (1996).
5) Yamada, A. and Tanaka, M., *Mater. Res. Bull.*, Vol. 30, pp. 715–721 (1995).
6) Rousse, G., Masquelier, C., Rodríguez-Carvajal, J. and Hervieu, M., *Electrochem. Solid-State Lett.*, Vol. 2, pp. 6–8 (1999).
7) Shimakawa, Y., Numata, T. and Tabuchi, J., *J. Solid State Chem.*, Vol. 131, pp. 138–143 (1997).
8) Oikawa, K., Kamiyama, T., Izumi, F., Chakoumakos, Bryan C., Ikuta, H., Wakihara M., Li J. and Matsui, Y., *Solid State Ionics*, Vol. 109, pp. 35–41 (1998).
9) Yamaguchi, H., Yamada, A. and Uwe, H., *Phys. Rev.*, B Vol. 58 pp. 8–11 (1998).
10) Rodríguez-Carvajal, J., Rousse, G., Masquelier C. and Hervieu, M., *Phys. Rev. Lett.*, Vol. 81, pp. 4660–4663 (1998).
11) Shiraishi, Y., Nakai, I., Tsubata, T., Himeda, T. and Nishikawa, F., *J. Solid State Chem.*, Vol. 133, pp. 587–590 (1997).
12) Ishizawa, N., du Boulay, D., Hayatsu, M., Kuze, S., Matsushima, Y., Ikuta, H., Wakihara, M., Tabira, Y. and Hester, J. R., *J. Solid State Chem.*, Vol. 174, pp. 167–174 (2003).
13) Tateishi, K., du Boulay, D., Ishizawa, N. and Kawamura, K., *J. Solid State Chem.*, Vol. 174, pp. 175–181 (2003).
14) Tateishi, K., du Boulay, D. and Ishizawa, N., *Appl. Phys. Lett.*, Vol. 84, pp. 529–531 (2004).
15) Verhoeven, V. W. J., de Schepper, I. M., Nachtegaal, G., Kentgens, A. P. M., Kelder, E. M., Schoonman J. and Mulder, F. M., *Phys. Rev. Lett.*, Vol. 86, pp. 4314–4317 (2001).
16) Suzuki, K., Oumi, Y., Takami, S., Kubo, M., Miyamoto, A., Kikuchi, M., Yamazaki, N. and Mita, M., *Jpn. J. Apll. Phys.* Vol. 39, pp. 4318–4322 (2000).
17) Tachibana, M., Tojo, T., Kawaji, H., Atake, T., Morita, N., Ikuta, H., Uchimoto, Y. and Wakihara, M., *J. Therm. Anal. Cal.*, Vol. 69, pp. 997–1004 (2002).
18) Kawamura, K., MXDORTO, Japan Chemistry Program Exchange, #026, private communication (2001).
19) Ida, Y., *Phys. Earth Planet. Inter.*, Vol. 13, pp. 97–104 (1976).
20) Verlet, L., *Phys. Rev.*, Vol. 159, pp. 98–103 (1967).
21) Ewald, P. P., *Ann. Phys.* Vol. 64, pp. 253–287 (1921).
22) Baur, W. H., *Acta Cryst. Sect. B*, Vol. B30, pp. 1195–1215 (1974).
23) Shannon, R. D., *Acta Cryst. Sect. A*, Vol. A32, pp. 751–767 (1976).